Modal analysis of jet near-field pressure fluctuation

Jean-Philippe Brazier, Maxime Huet, Olivier Léon, Maxime Itasse

MODAL ANALYSIS OF JET NEAR-FIELD PRESSURE FLUCTUATION

J.-Ph. Brazier[1], M. Huet[2], O. Léon[1], M. Itasse[1]

[1]: DMAE, Université Fédérale de Toulouse, ONERA, Toulouse, France

[2]: DAAC, ONERA, Châtillon, France

Abstract

Purpose

Unstable Kelvin-Helmholtz waves are suspected to be responsible for a large part of low-frequency noise radiation in high-speed jets. The purpose of this paper is to check the coherence of several numerical and experimental data concerning this phenomenon, in the particular case of a cold subsonic jet.

Design/methodology/approach

In the present work, a cross investigation of the near pressure field is performed on three different data sets: LES computations, PSE semi-modal computations and microphone measurements, in order to determine the local amplitudes of unstable waves.

Findings

The large coherent structures are found in both LES and experimental results and they are also in good agreement with direct semi-modal computations carried out with the PSE approach.

Originality/value

This work confirms that the unstable wave packets can be extracted from both LES and experimental results, provided that an appropriate modal decomposition is performed.

Keywords jet noise, LES, instability, PSE, POD

Paper type Research paper

Nomenclature

D	nozzle diameter
PSD	power spectral density
f	frequency
m	azimuthal wavenumber
M_j	Mach number in the centre of the nozzle exit section
p	pressure fluctuation
r	radial coordinate
R	radius of the cylindrical surface
SPL	sound pressure level
St	Strouhal number
t	time
T_j	static temperature in the centre of the nozzle exit section
U_j	axial velocity in the centre of the nozzle exit section
U_x	axial velocity for the jet base flow
x	axial coordinate
α	axial wavenumber
ω	angular frequency

1. Introduction

Understanding the physical mechanisms of jet noise has been the subject of many works and articles for several decades and in spite of important progress in both experimental and numerical domains, this topic is still relevant. In particular, beside small-scale chaotic turbulence, large-scale coherent structures have been observed in jets mixing layers (Crow and Champagne, 1971). These large coherent structures are generated by Kelvin-Helmholtz instability waves which are amplified at the nozzle exit, due to the strong shear in the mixing layer, and then damped further downstream (Tam and Burton, 1984). They can be represented as wave packets of limited axial extent. Their role in the generation of directional low-frequency noise is more and more suspected, according to theoretical modelling as well as experimental investigation (Suzuki and Colonius, 2006). A good review can be found in the recent article by Jordan and Colonius, 2013. If the acoustic radiation of supersonic jets can explained by a mechanism based on Mach waves (Troutt and McLaughlin, 1982), the extension to subsonic jets is not obvious. However, it has been shown in recent works that the sound directivity of a subsonic jet could be favourably compared with the acoustic radiation of a model wave packet (Cavalieri *et al.*, 2012). In hot subsonic jets, due to the temperature ratio between the jet and the ambient medium, some coherent structures can be convected at supersonic speeds with regard to the outer sound celerity. In this case, the sound radiation mechanism is similar to that of supersonic jets. But this cannot be invoked for cold subsonic jets and the first purpose of the present work was to investigate particularly the pressure near-field of such a cold subsonic jet, in order to feed a future acoustic investigation.

Derived from linearised Euler or Navier-Stokes equations, the Parabolised Stability Equations (PSE) can be seen as an extension of the local linear stability approach, since they can take into account the slow axial variation of the base flow, and they constitute an efficient way to compute the axial evolution of an unstable wave packet. They were first derived to compute boundary-layer instabilities (Herbert, 1997) and then applied to jets (Yen and Messersmith, 1998, Balakumar, 1998). A close agreement between PSE results and near-field pressure measurements made with circular antennas was reported (Gudmundsson and Colonius, 2011). However, the far-field acoustic radiation cannot be directly provided by the PSE solution and an extrapolation with a Kirchhoff integral formula is required (Balakumar, 1998). Dual-stream jets were also investigated (Léon and Brazier, 2013). The PSE can also be extended to deal with weakly nonlinear interactions between unstable modes (Itasse *et al.*, 2015 and references included).

In the framework of the ORINOCO project, carried out in cooperation between European and Russian laboratories, concurring computations and experiments were performed on a cold subsonic jet. Using three different numerical and experimental data sets collected at ONERA during this project, it is possible to explore the near pressure field of this jet and to verify that the signature of the large coherent structures can be extracted from measurements and correctly predicted by computations. This is the second purpose of the present paper.

2. Experiment

2.1. *Experimental setup*

The cold subsonic jet investigated during the ORINOCO project was produced by a circular nozzle of diameter D = 50 mm. The geometry of this nozzle had been formerly designed during the European project JEAN and the nozzle lip has been thickened to 15 mm to integrate plasma actuators. In the present case, only the unforced jet is considered. In the exit section, the flow on the nozzle axis is characterised by a Mach number M = 0.85, an axial velocity U_j = 292 m/s and a static temperature T_j = 296 K. Outside of the jet, the parameters of the quiet air are a pressure of 1 atm and a temperature of 295 K, giving a sound speed of 344 m/s.

In the following, the frequency will often be replaced by the dimensionless Strouhal number, defined as

$$St = \frac{f\,D}{U_j} \tag{1}$$

where D is the nozzle diameter. The instabilities of a circular jet are typically encountered for Strouhal values between 0.1 and 0.9, with a maximum near 0.4. In the case of the present jet, it corresponds to frequencies roughly lying between 600 Hz and 5000 Hz.

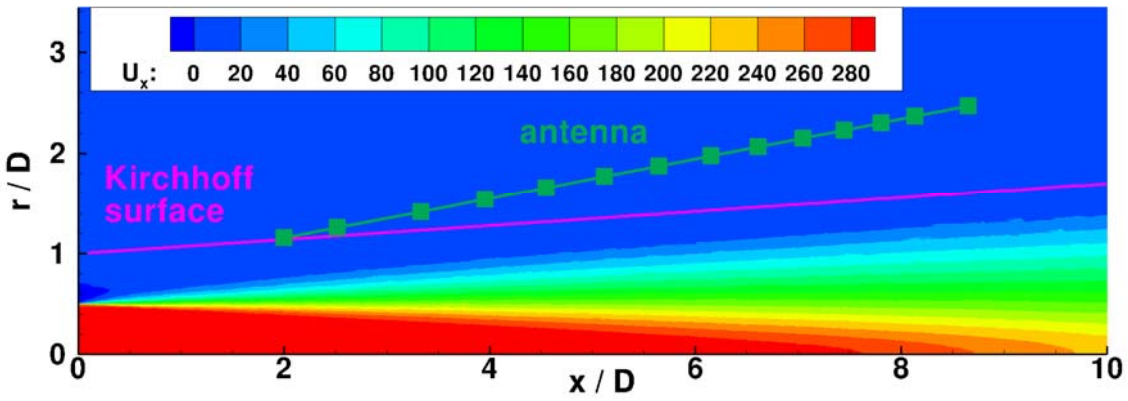

Figure 1. Computed mean flow field and linear microphone array

2.2. *Measurement setup*

Several measurement techniques were used to investigate both the mean flow field and the fluctuating part of this jet. First, the mean velocity field was measured with a two-component PIV system in the axial sections. The PIV system was composed of a MotionPro X5 camera of 2352 x 1728 px resolution mounted with a 50 mm lens, and a double-pulsed Nd:YAG Quantel laser of 150 mJ per pulse. The system was operated at a repetition rate of 4 Hz, with an inter-pulse period of 2 µs. Atomized DEHS oil, providing droplets with a mean diameter less than 1 µm, was employed to seed the flow. The seeding was introduced upstream of the jet exit, at about 30 D and before the flow rectifier located in the air-supplying pipe. This ensured a homogeneous seeding in the jet core. Furthermore, seeding was also introduced around the exit plane, at very low velocities, in order to seed the surrounding air dragged along by the jet. In order to accurately measure the entire flow field up to 10 D downstream, the PIV system was mounted on a traverse system and a set of eight spatial windows was acquired with overlaps. For each acquisition window, a total of 400 pairs of images was acquired, which was observed to be sufficient to provide well-converged first and second-order moment statistics. Post-processing was performed based on a classical cross-correlation technique using LaVision's Davis software, with interrogation windows of 16 px x 16 px, leading to a spatial resolution of 0.81 mm.

Then, near-field pressure fluctuations were recorded using a linear microphone array located close to the jet axis (Figure 1). This array had 14 microphones and formed an angle of 11 degrees with the jet axis. The first microphone was located at an abscissa x = 2 D and a radius r = 1.15 D. In this way, the array was located in the linear-hydrodynamic region (Suzuki and Colonius, 2006), where the pressure fluctuations are dominated by the instability waves, whereas farther from the jet, the pressure fluctuations are driven by the acoustic field only. The sampling frequency was 48 kHz.

3. Navier-Stokes computations

3.1. *Mean flow computation*

Before performing the PSE analysis, the jet mean flow field must be computed. This was done using ONERA code *CEDRE*, which solves the Navier-Stokes equations on an unstructured grid with a finite-volume formulation. The steady solution (Figure 1) was obtained by a RANS computation using a *k-l* turbulence model on a three-dimensional grid corresponding to a 15 degrees angular sector. The full grid was composed of 2.2 x 10^6 elements; the fluid volume was discretized with tetrahedra while prisms were used at the nozzle wall to capture the turbulent boundary-layer, together with a turbulent wall-law model. Special care was given to the resolution of the flow gradients in the shear layer with the use of very small elements. Spatial discretization was performed with a second-order MUSCL scheme and time integration was achieved with a first-order implicit scheme, allowing the use of a large time step to fasten the convergence of the mean flow. Finally, inlet turbulent parameters were tuned to best fit the experimental results and the values imposed at nozzle inlet were $k = 5\ m^2.s^{-2}$ and $l = 0.005$ m. They correspond to a homogeneous isotropic turbulence with velocity fluctuations amplitudes being 3% of the mean inlet velocity and a length scale of $1/20^{th}$ of the inlet boundary diameter. As it was not possible to recover with the simulation both the potential core length and the correct downstream axial velocity decrease provided by PIV, a dilatation coefficient had to be applied to the axial coordinate in the computation. The turbulence level in the nozzle exit section has been tuned in such a way that after dilatation, the length of the potential core and the decrease of the velocity on the jet axis both agreed with experiment (Figure 2). A satisfying agreement was also observed between computation and PIV measurements on the radial profiles of axial velocity, which is mandatory for shear layer instability calculations.

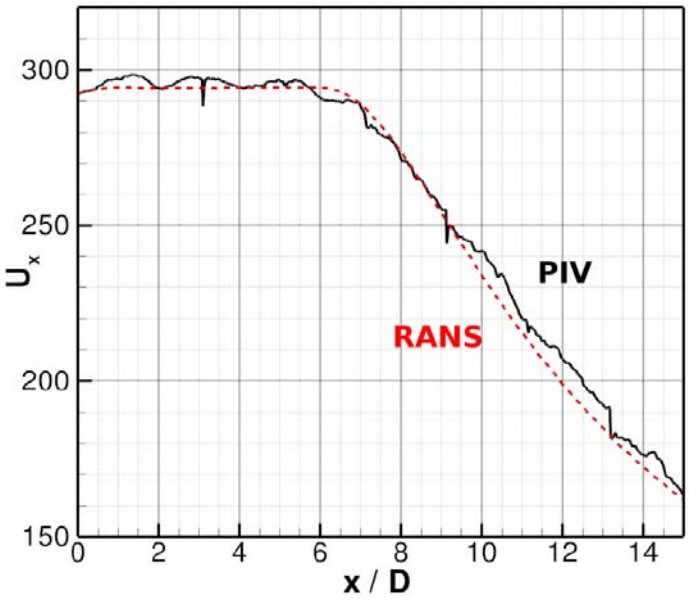

Figure 2. Axial velocity evolution along the jet axis

3.2. *Large-Eddy Simulation*

The unsteady jet simulation was also performed with CEDRE. A second-order scheme was used for the spatial discretization, together with a first-order implicit scheme for time integration. A Smagorinsky subgrid-scale model represented the filtered structures in the frame of Large-Eddy Simulation (LES).

Simulations have been performed with a time step $\Delta t = 3\times10^{-7}$ s which ensured a CFL number lower than 1 in almost all the numerical domain. After a transient period of 24 ms (80,000 iterations) required to let the jet flow develop, the simulations were run for 234,000 iterations to perform mean flow averaging and far-field noise radiation. It corresponds to a physical time of 70.20 ms or to a non-physical time of 420 convective time units D / Uj. Previous simulations of a similar case (Huet *et al.*, 2012) have demonstrated that this duration is sufficient to provide a statistical convergence of the flow fields and far-field pressure spectra.

The grid has been shown to be fine enough to accurately propagate acoustic waves at least up to a Strouhal number of 1.15 (corresponding to a frequency of 7000 Hz) with 30 points per wavelength. To ensure a convenient turbulence level in the nozzle exit section, the turbulence must be triggered in the nozzle internal boundary-layer. This was done through a geometrical disturbance of the nozzle inner wall, from x / D = -0.9 to x / D = -0.5, with an amplitude of ± 0.02 D (1 mm).

For data post-processing, the time results were stored on several cylindrical or conical surfaces. One of them was intended for Kirchhoff integral extrapolation of the acoustic far field, which will not be presented here. Its position is shown in Figure 1. Unfortunately, it does not coincide with the position of the linear antenna, but PSE computations will make possible some comparisons between both surfaces. A more detailed presentation of the unsteady simulations and associated results is available in (Huet, 2014).

4. PSE computations

The Parabolised Stability Equations (PSE) approach has been widely applied first to boundary-layer instability and then to jet instability (Gudmundsson and Colonius, 2011; Léon *et al.*, 2013). This method can be employed to describe wave propagation in flows with a strong transverse variation and a slow axial evolution, which is the case for circular jets. Starting from linearised perturbation equations, the time and azimuthal dependences are expressed through an exponential term whereas the axial evolution is split in two parts, according to the scheme:

$$\phi'(x, r, \theta, t) = \hat{\phi}(x, r) \, . \, e^{im\theta - i\omega t} \, . \, e^{A(x)} \tag{2}$$

with $A(x) = \int_0^x i\alpha(\xi)d\xi$.

In the above expression, ω represents the angular frequency and m is the integer azimuthal wave number. The real part of the complex parameter α represents the local axial wave number whereas the imaginary part of α is the opposite of the local amplification rate. In this way, all the rapid phase fluctuations and the exponential growth should be included in A(x) and therefore the amplitude function $\hat{\phi}$ should only exhibit slow variation in the axial direction. The introduction of α must be compensated by a closure relation called the normalisation condition. This relation is not unique but the most common one will be used in the present work:

$$\int_0^\infty \hat{\phi}^* \frac{\partial \hat{\phi}}{\partial x} dr = 0 \tag{3}$$

For jet instability, the viscosity does not play a key role and it can be neglected as a first step. The above decomposition (Eq. 2) is thus introduced in Linearised Euler Equations, with prescribed frequency and azimuthal wave number. The resulting set of equations can be shown to be quasi-parabolic in the axial direction and therefore, due to the slow evolution of the amplitude variables, it can be integrated at low computational cost by a marching procedure with a large step size. At each step, the normalisation condition (Eq. 3) is solved iteratively. The initial solution at x = 0 is provided by a local stability analysis. For linear PSE computations, the initial amplitude is arbitrary and it is fixed by imposing the maximum of pressure fluctuation equal to unity. The true amplitude level will be determined later by comparison with LES or experimental results.

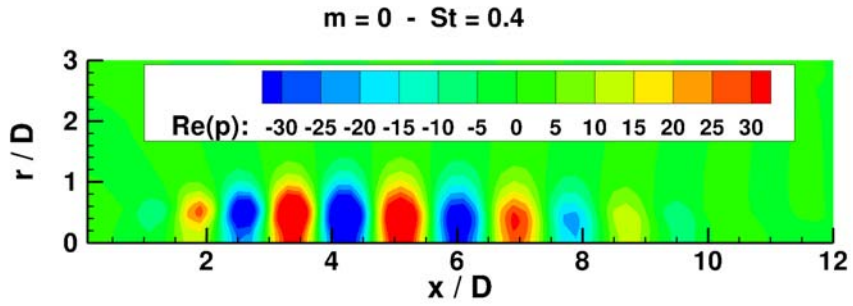

Figure 3. PSE pressure fluctuation field – m = 0 – St = 0.4

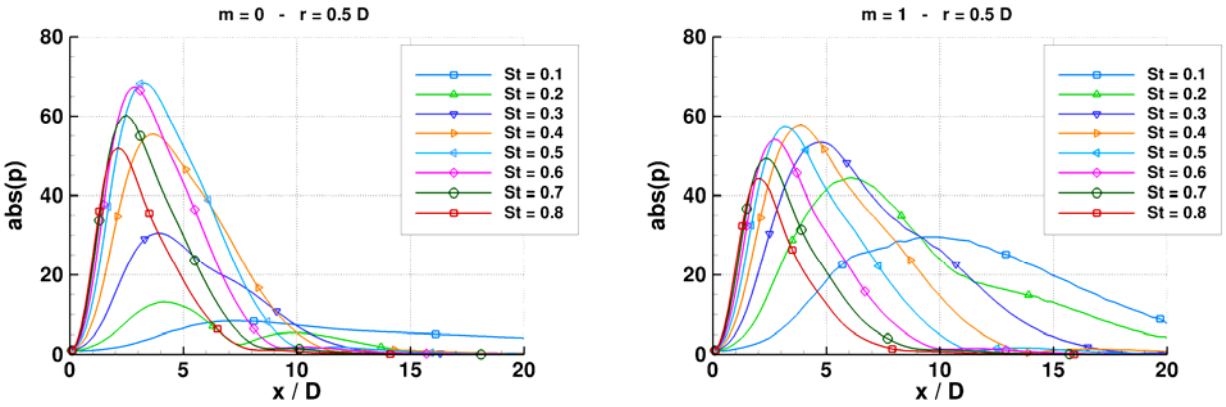

Figure 4. PSE pressure fluctuation amplitude for r = 0.5 D – m = 0 (left) and m = 1 (right)

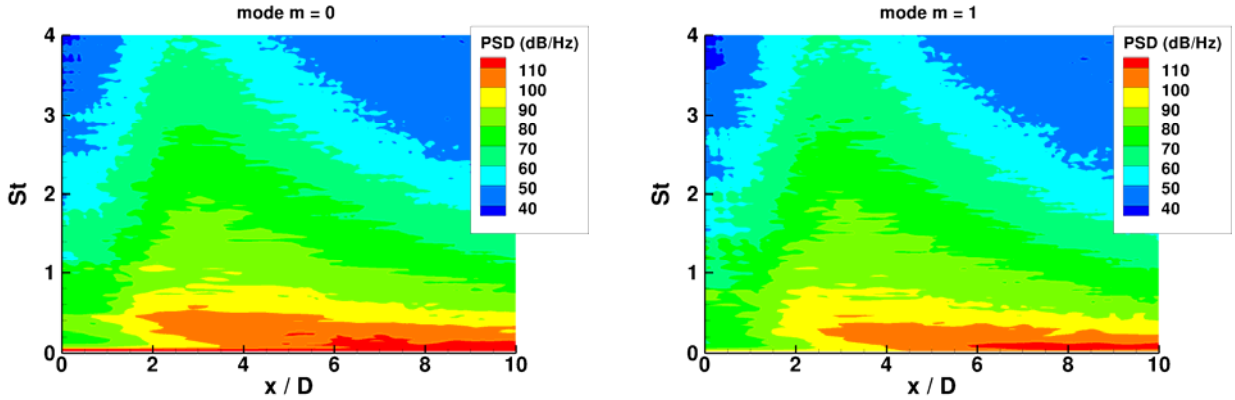

Figure 5. LES power spectral density for the pressure fluctuation on the conical surface

An example of pressure fluctuation field predicted by PSE computation for m = 0 and St = 0.4 is shown in Figure 3. The shape of the wave packet appears clearly, with an axial extent roughly equivalent to three wave lengths. The wave is first amplified, then damped when the mixing layer thickness has increased. The amplification of the different frequencies is summarised in Figure 4 for m = 0 and m = 1. The pressure amplitude has been plotted for a fixed radius r = 0.5 D corresponding to the nozzle lip. All the waves start with unit amplitude at x = 0.1 D. The frequencies of the most amplified waves lie between St = 0.4 and St = 0.8 and the axisymmetric mode m = 0 is slightly more amplified than the first helical mode m = 1.

5. Comparison of LES and PSE results

5.1. *Processing of LES results*

The amplitude of pressure fluctuations predicted by LES and PSE approaches will be compared along the line representing the Kirchhoff's surface (Figure 1). First, the temporal LES results have been processed with a double Fourier transform on both time and azimuthal coordinates. The diagram of power spectral density for the pressure fluctuation given by LES on the Kirchhoff's conical surface is plotted in Figure 5 for azimuthal wave numbers m = 0 (left) and m = 1 (right). It can be observed that except for very low frequencies, the power density increases until x / D close to 3 and then decreases. The maximum is obtained for Strouhal numbers between 0.2 and 0.6, which corresponds roughly to the range of the most

linearly amplified modes (Figure 4). Moreover, the density is slightly higher for m = 0 than for m = 1. The high levels on low frequencies past x / D = 5 may be due to insufficient statistical convergence of the LES downstream, caused by the limited time length of the simulation.

Figure 6 shows the repartition of the power between azimuthal modes for a fixed frequency, corresponding to St = 0.4, still along the conical surface. The comparison between positive and negative helical modes, which should have the same level, gives an appraisal of the precision of the results. Up to x / D = 4, the axisymmetric mode dominates and modes with |m| > 2 are far lower.

5.2. *PSE modes fitting on LES results*

From now on, the amplitudes are plotted in dB logarithmic scale and therefore a multiplicative coefficient on the initial amplitude corresponds to a vertical translation of the curves. The pressure fluctuations along the conical surface are plotted for Strouhal numbers from 0.3 to 0.6 and for azimuthal wave numbers m = 0 and m = 1 in Figures 7 and 8. In these cases, the initial exponential growth and the maximum of fluctuation are very well reproduced by the PSE solutions, but downstream they decrease strongly whereas the LES levels exhibit constant or slowly decreasing values. A possible explanation to this difference will be proposed in the next paragraph when a comparison between PSE and experimental levels will be proposed.

The same kind of results has been obtained on the other cylindrical surfaces R = 0.3 D, 0.5 D and 1.2 D where LES data were also stored, but they will not be all presented here. An example of amplitude adjustment for the PSE on the cylindrical surface R = 0.5 D is shown in Figures 14 and 15 in the Appendix. The important fact is that the initial amplitude of a given PSE mode remains of the same order of magnitude when LES and PSE data are fitted on different surfaces.

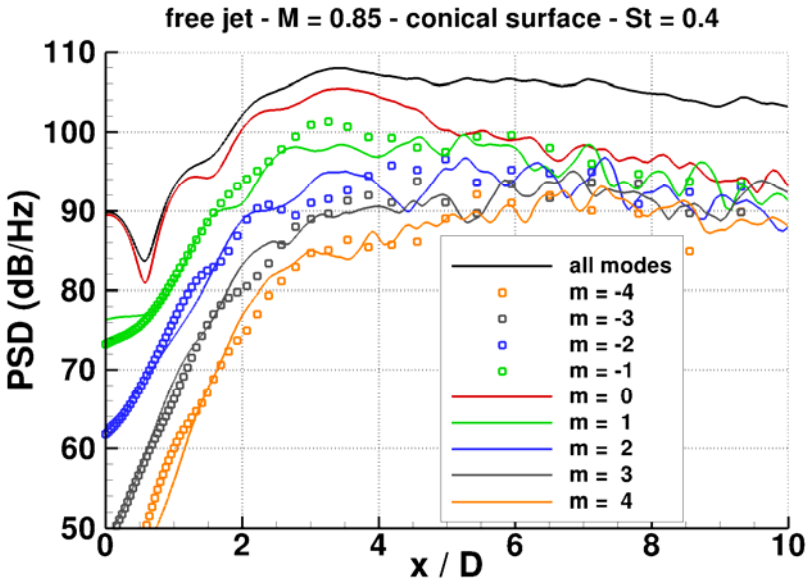

Figure 6. LES power spectral density for St = 0.4

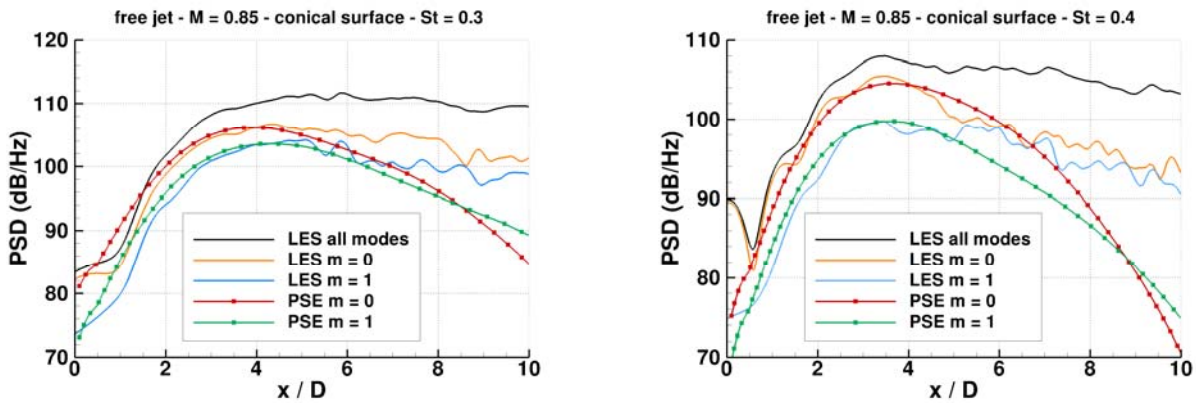

Figure 7. PSE modes amplitude adjustment on LES results – St = 0.3 (left) and St = 0.4 (right). Conical surface

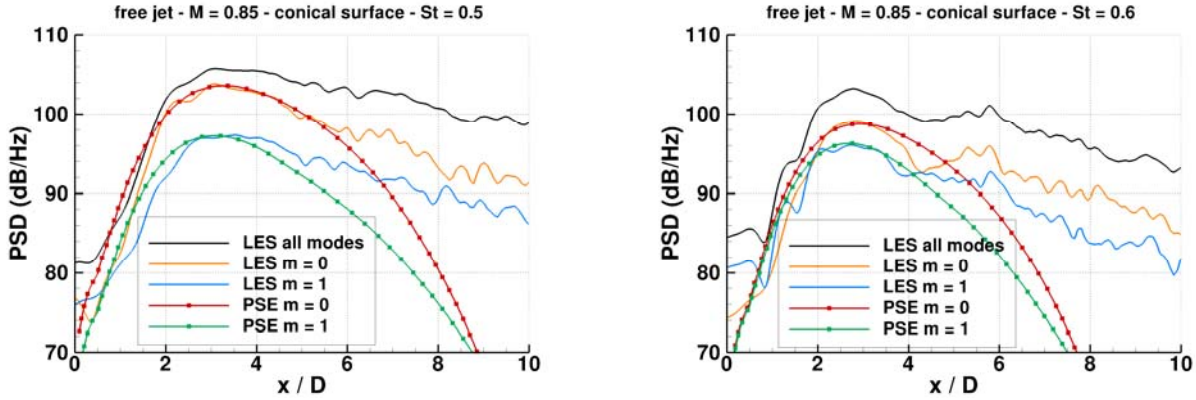

Figure 8. PSE modes amplitude adjustment on LES results – St = 0.5 (left) and St = 0.6 (right). Conical surface

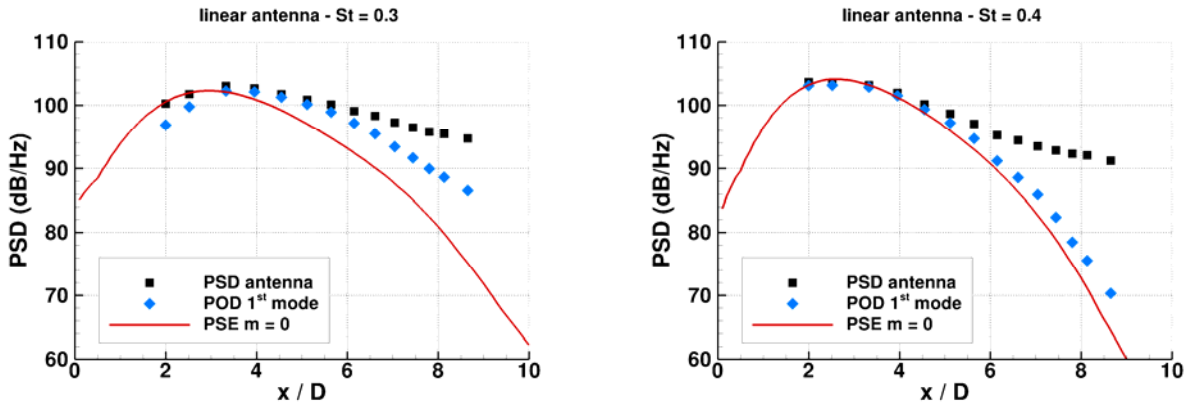

Figure 9. PSE modes amplitude adjustment on measurements – St = 0.3 (left) and St = 0.4 (right)

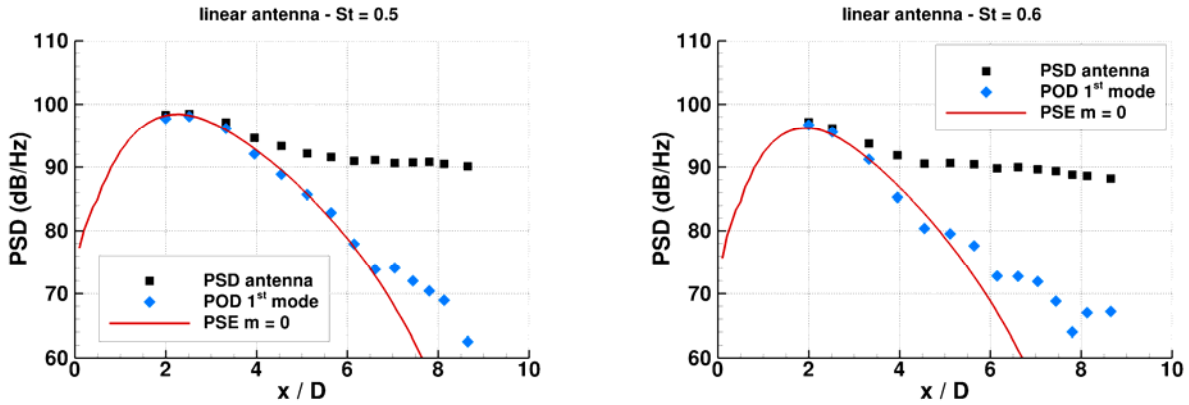

Figure 10. PSE modes amplitude adjustment on measurements – St = 0.5 (left) and St = 0.6 (right)

6. Comparison of PSE and measured data

PSE amplitudes are now fitted on experimental values measured with the linear antenna (Figure 1). First, the Power Spectral Density (PSD) has been computed in the frequency domain for each microphone. A circular antenna would have been necessary to provide information on the azimuthal structure of the pressure fluctuations, but such a device was unfortunately not available. However, in the LES data set, the axisymmetric mode $m = 0$ has been seen to dominate the helical modes in the first part of the jet. Therefore, as a first approximation, the PSE axisymmetric mode alone will be compared to the measurements.

Moreover, since all the microphones have been recorded simultaneously, it has been possible to perform a Proper Orthogonal Decomposition (POD) on the antenna signal. This statistical analysis allows to isolate the most coherent structures in the axial direction. In this way, the adjustment of PSE amplitudes on experimental values is shown in Figures 9 and 10 for Strouhal numbers from 0.3 to 0.6. It appears that the first microphone is located too much downstream to provide information on the exponential growth phase of the modes, close to the nozzle. However, the first POD mode compares favourably with the decrease stage of the PSE mode, whereas the global PSD of the antenna stagnates or decreases slowly, in the same way that was observed for LES data in the previous paragraph. Applying the same POD algorithm to the previous LES results would perhaps allow to isolate axially coherent structures with a decrease slope closer to that of the PSE modes.

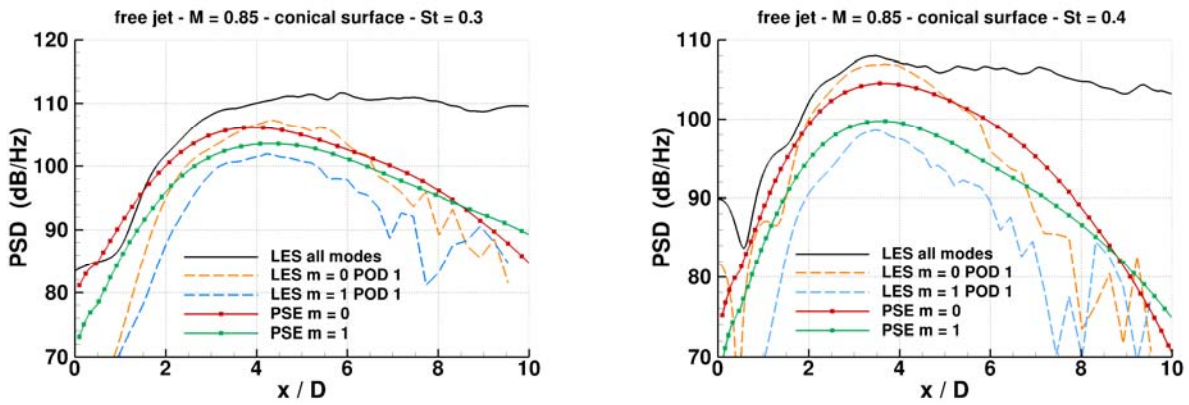

Figure 11. PSE modes versus 1st POD modes of LES – St = 0.3 (left) and St = 0.4 (right)

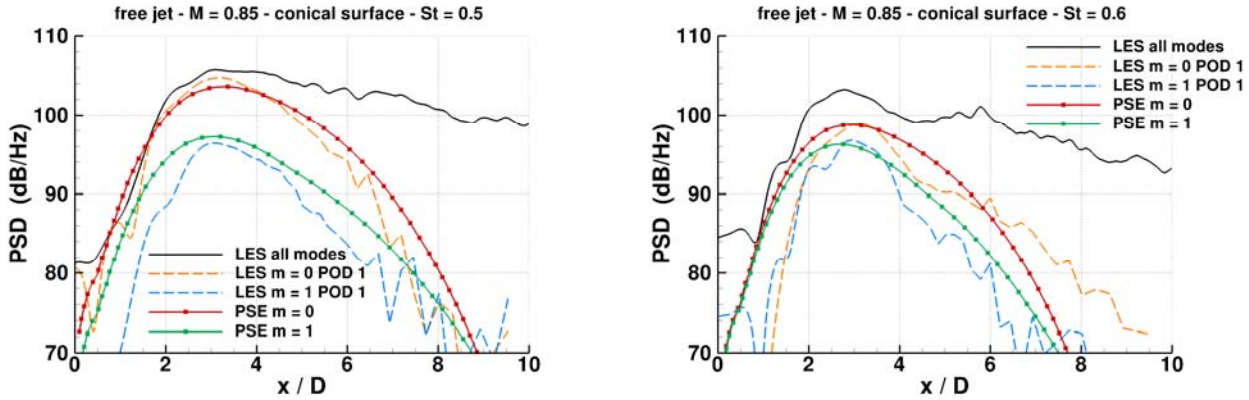

Figure 12. PSE modes versus 1st POD modes of LES – St = 0.5 (left) and St = 0.6 (right)

This has been carried out for the LES data on the conical surface. The first axial POD modes computed from LES results are plotted in Figures 11 and 12, together with PSE results, for Strouhal numbers from 0.3 to 0.6 and for the azimuthal wave numbers m = 0 and m = 1. Obviously, the POD method applied to LES results does not provide smooth results, particularly downstream of x/D = 6. This was already observed on azimuthal decomposition (Figures 6 to 8) and it is probably due to an insufficient time convergence of the computation in this region. However, the strong decrease of the first POD modes is comparable to that of PSE curves and it is probably representative of a physical phenomenon since the same tendency is observed on experimental results (Figures 9 and 10). This qualitative result should be confirmed with more accurate LES simulations.

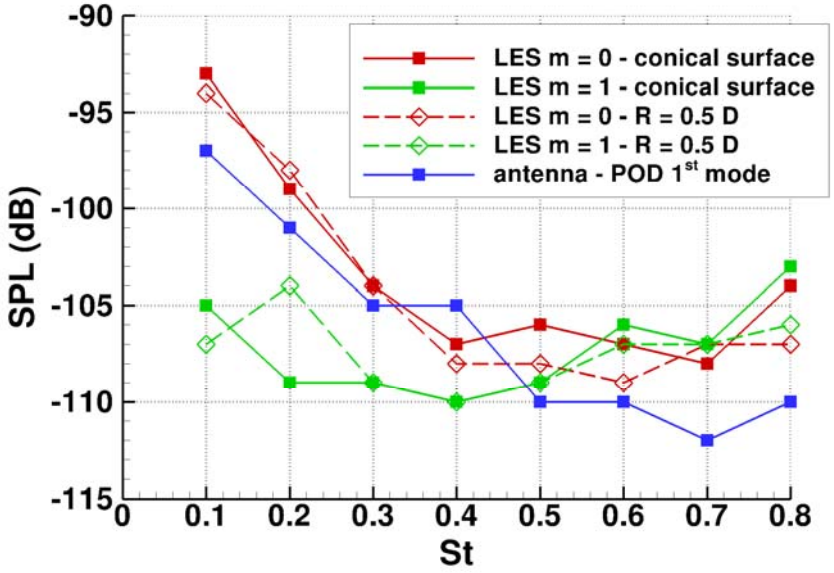

Figure 13. Comparison of absolute amplitudes of the PSE modes fitted on LES or experimental results

7. Comparison of experimental and measured amplitudes

The comparison of the absolute amplitudes of PSE modes fitted on LES and experimental data is summarized in Figure 13. The scale is in decibels for the sound power level, in dimensionless variables. Thus a level of -100 dB corresponds to a dimensionless amplitude of 10^{-5} for the PSE pressure fluctuation at the abscissa x = 0.1 D where the PSE solution starts. The amplitudes deduced from LES results on the conical surface, located outside of the jet, are first compared to the amplitudes deduced from LES data on a cylindrical surface R = 0.5 D, corresponding to the nozzle lip. These values are relatively close, for both m = 0 and m = 1, showing that the pressure fluctuations inside and outside of the jet can be represented by the same mode. At low frequency, the axisymmetric mode m = 0 has a larger amplitude than the first helical mode m = 1, but at higher frequencies both modes have a similar initial amplitude.

Considering the absolute amplitude deduced from the first POD mode of the linear antenna, it remains close to the values of the axisymmetric mode for frequencies up to St = 0.6 and slightly lower for higher frequencies. It is reminded that this value has been obtained without separation of the azimuthal modes and therefore it is more significant when only the axisymmetric mode dominates. Nevertheless, one order of magnitude on the amplitude of the pressure fluctuation corresponds to 20 dB on this graph and thus it can be stated that the LES is able to predict the correct order of magnitude of the pressure fluctuations. Moreover, this order of magnitude does not vary significantly with the frequency, in the considered range.

8. Conclusion

Based on three different data sets originating from numerical LES, semi-modal PSE approach and near-field pressure fluctuation measurements, a cross-comparison has been performed with the aim to get further insight on the existence and on the properties of large coherent structures in turbulent high-speed jets. Beside heavy numerical simulations like LES, the PSE approach is well suited to track the unstable modes developing in the jet shear layer. The evolution of these unstable modes directly predicted by the PSE exhibits strong similarities with results provided by the other approaches, giving a great presumption that they all describe the same physical phenomenon. However, before making this comparison possible, both LES and experimental results must undergo an appropriate modal decomposition along the three main

coordinates, *i.e.* a Fourier decomposition in time and in azimuthal angle and a POD analysis in the axial direction. This analysis allows to isolate what seems to be the right mode corresponding to PSE results. This also confirms previous results published by several research teams. One key contribution of the present work is to confirm that the results obtained when performing the analysis at different radial positions remain coherent between LES and PSE. The radial structures of the PSE modes and of the modes extracted from LES are therefore very close. The PSE approach also allows to compare LES and experimental values when the data are not stored at the same position, which is the case in the present work.

Further investigations should however be done, like an improvement of the time convergence of the LES computation at greater axial positions, or an experimental investigation of the radial and azimuthal structures of the near-field pressure fluctuations. Using circular microphone arrays could give an insight on the azimuthal decomposition of the experimental pressure fluctuations. Moreover, recent works in progress in other laboratories take advantage of the Time-Resolved PIV to investigate the radial structure of the near-field velocity fluctuations, which could be fruitfully compared to PSE solutions. Beside POD also exist other statistical techniques of modal decomposition, like Dynamical Mode Decomposition (DMD), which could be tested on the present numerical and experimental data. The question of understanding the physical nature of the fluctuations developing downstream of the potential core and represented by the higher-order axial POD modes, that is: everything except the basic Kelvin-Helmholtz mode, also requires a particular attention. Of course, the final objective of noise generation understanding will require far-field noise measurements together with far-field extrapolation of both LES and PSE solutions.

Acknowledgements

The ORINOCO project was granted by the European Union, as part of the 7th Framework Programme for Research and Technological Development, and by the Russian Government.

References

Balakumar, P. (1998), “Prediction of supersonic jet noise”, *AIAA Paper 98-1057, 36th AIAA Aerospace Sciences Meeting,* Reno.

Cavalieri, A.V.G., Jordan, P., Colonius, T., and Gervais, Y. (2012), “Axisymmetric superdirectivity in subsonic jets”, *Journal of Fluid Mechanics,* Vol. 704, pp. 388-420.

Crow, S.C. and Champagne, F.H. (1971), “Orderly structure in jet turbulence”, *Journal of Fluid Mechanics,* Vol. 48 No. 3, pp. 547-591.

Gudmundsson, K. and Colonius, T. (2011), “Instability wave models for the near-field fluctuations of turbulent jets”, *Journal of Fluid Mechanics,* Vol. 689, pp. 97-128.

Herbert, T. (1997), “Parabolized Stability Equations”, *Annual Review of Fluid Mechanics,* Vol. 29, pp. 245-283.

Huet, M., Rahier, G. and Vuillot, F. (2012), “Simulation of flow control with microjets for subsonic jet noise reduction”, in Colman Lerner, J. (Ed.), *Applied Aerodynamics*, InTech, ISBN: 978-953-51-0611-1, pp. 79-106, available at: http://www.intechopen.com/books/applied-aerodynamics/simulation-of-flow-control-with-microjets-for-subsonic-jet-noise-reduction.

Huet, M. (2014), “On the use of Plasma Synthetic Jets for the control of jet flow and noise”, *AIAA Paper 2014-2620, 20th AIAA/CEAS Aeroacoustics Conference,* Atlanta.

Itasse, M., Brazier, J.-Ph., Léon, O. and Casalis, G. (2015), “Parabolized Stability Equations analysis of nonlinear interactions with forced eigenmodes to control subsonic jet instabilities”, *Physics of Fluids,* Vol. 27, pp. 084106.

Jordan, P. and Colonius, T. (2013), “Wave packets and turbulent jet noise”, *Annual Review of Fluid Mechanics,* Vol. 45, pp. 173-195.

Léon, O. and Brazier, J.-Ph. (2013), “Investigation of the near and far pressure fields of dual-stream jets using an Euler-based PSE model”, *AIAA Paper 2013-2280, 19th AIAA/CEAS Aeroacoustics Conference,* 27-29 May, Berlin.

Suzuki, T. and Colonius, T. (2006), “Instability waves in a subsonic round jet detected using a near-field phased microphone array”, *Journal of Fluid Mechanics,* Vol. 565, pp. 197-226.

Tam, C.K.W. and Burton, D.E. (1984), “Sound generated by instability waves of supersonic flows. Part 2. Axisymmetric jets”, *Journal of Fluid Mechanics,* Vol. 138, pp. 273-295.

Troutt, T.R. and McLaughlin, D.K. (1982), “Experiments on the flow and acoustic properties of a moderate-Reynolds-number supersonic jet”, *Journal of Fluid Mechanics,* Vol. 116, pp. 123-156.

Yen, C.C. and Messersmith, N.L. (1998), “Application of parabolized stability equations to the prediction of jet instabilities”, *AIAA Journal,* Vol. 36 No. 8, pp. 1541-1544.

Appendix

The graphs representing the adjustment of the absolute amplitude of the PSE solutions on the LES values for the cylindrical surface R = 0.5 D, corresponding to the position of the nozzle lip and therefore to the centre of the shear layer, are presented in Figures 14 and 15. These plots can be directly compared to those of Figures 7 and 8 corresponding to the conical surface. In the case of the cylindrical surface, the decay occurs later than for the conical surface, where the maximum of fluctuation has a shorter axial extent. The initial amplitudes issued from both surfaces are compared in Figure 13.

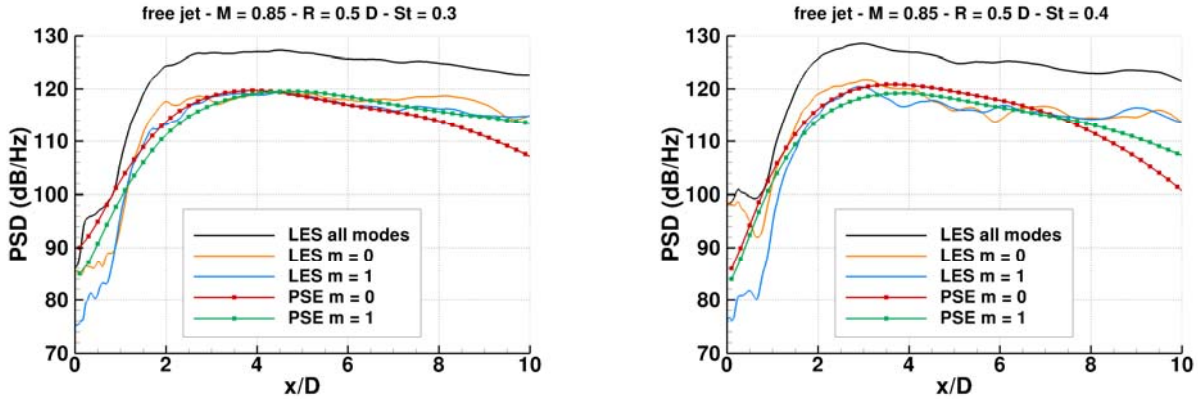

Figure 14. PSE modes amplitude adjustment on LES results – St = 0.3 (left) and St = 0.4 (right). Cylindrical surface R = 0.5 D

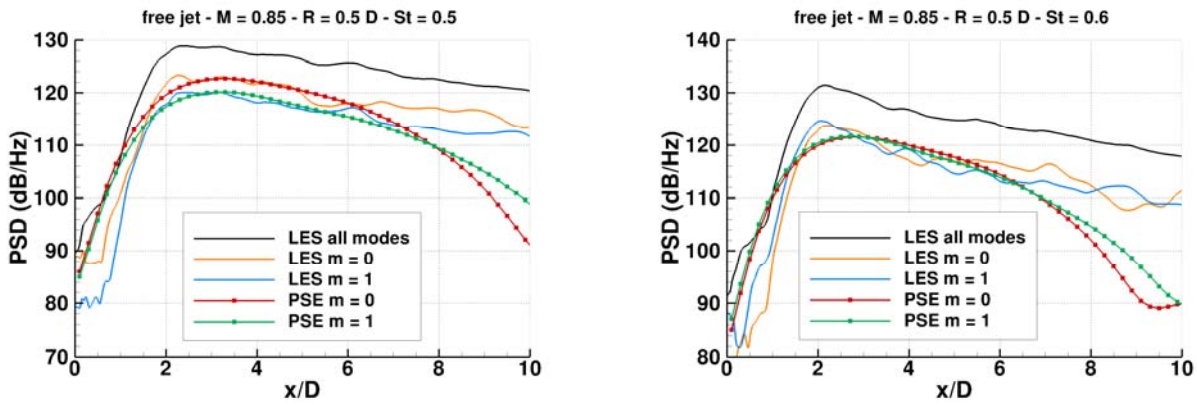

Figure 15. PSE modes amplitude adjustment on LES results – St = 0.5 (left) and St = 0.6 (right). Cylindrical surface R = 0.5 D